PROCEEDINGS, 41st Workshop on Geothermal Reservoir Engineering
Stanford University, Stanford, California, February 22-24, 2016
SGP-TR-209

Passivation of metal surfaces against corrosion by silica scaling

Daniela B. van den Heuvel[1], Einar Gunnlaugsson[2], Liane G. Benning[1,3]

[1]Cohen Geochemistry Group, School of Earth and Environment, University of Leeds, Leeds LS2 9JT, United Kingdom;

[2]Reykjavik Energy, Baejarhals 1, 110 Reykjavik, Iceland

[3]German Research Center for Geosciences, GFZ, 14473, Potsdam, Germany

Email: eedbm@leeds.ac.uk, liane.g.benning@gfz-potsdam.de

Keywords: silica, scaling, corrosion

ABSTRACT

In high-enthalpy geothermal systems the precipitation of amorphous silica (SiO_2) is the most common scaling problem. Together with corrosion, silica scaling affects the efficiency of geothermal power plants through increased maintenance costs and reduced equipment lifetimes. Despite their crucial importance for the development of better mitigation strategies, the relationship and inter-dependencies between scaling and corrosion are poorly understood. Here we present data from a time resolved study where the development of both silica precipitates and corrosion features on S316 stainless plates and S275 carbon steel coupons immersed in geothermal waters at the Hellisheiði power plant (SW-Iceland) were followed for between 1 day and 10 weeks. We chose four locations that differ with respect to fluid temperatures (55 to 120 °C) and silica concentration (550 to 800 mg/L) and characterized the morphologies and textures of the precipitating silica and the corrosion products by high resolution imaging, while the solid precipitates and corrosion products were identified by X-ray diffraction (XRD) and energy dispersive spectroscopy (EDS). Silica precipitates were observed on all plates as uneven layers and rounded 'bumps' covering the plates completely, even after 1 day. With time and regardless of prevailing conditions, the size of the individual 'bumps' increased. Where silica precipitation was high, the carbon steel revealed only minor signs of corrosions, while where silica precipitation was minor ubiquitous corrosion was observed. The corrosion products were composed of iron sulfides (mackinawite and greigite), as well as their oxidized products (elemental sulfur, goethite and hematite). We show that in environments where silica precipitation is slow, corrosion dominates, while once an initial amorphous silica layer formed fast this will protect the underlying carbon steel from further reaction with the geothermal fluids and therefore from continuing corrosion. Thus, silica scaling can indeed act as a passivating agent for steel surfaces prone to corrosion.

INTRODUCTION

Geothermal fluids are often rich in dissolved solids and gases, leading to two challenges which have to be overcome in order to run a high enthalpy geothermal power plants efficiently: scaling, i.e., the unwanted precipitation of minerals inside pipelines and other fluid-handling equipment, and corrosion. Both of these processes can result in the clogging of pipelines, heat exchangers and wells and reduce the lifetime of pumps and turbines. They also impair the financial performance of a power plant due to the reduction in power generation, increased operating costs (e.g., additional costs for anti-scaling treatments or more corrosion-resistant additives or need for additional pumping capacity) and longer and more regular downtimes required for cleaning and maintenance of the system.

In the high-enthalpy systems of Iceland, the biggest challenge is amorphous silica scaling (Gunnarsson and Arnórsson, 2003). Silica is very abundant in most geothermal waters with concentrations of more than 1200 ppm SiO_2 in the geothermal fluids of the Hengill area, Iceland (Scott et al., 2014). Once silica supersaturation is reached, precipitation, especially under conditions of high ionic strength, was observed to be very rapid with rates of over 300 kg $year^{-1}$ m^{-2} in the wastewater drains at the Reykjanes geothermal field (Tobler et al., 2008). Silica scales can also be very hard and are not easily dissolved and therefore difficult to remove from equipment surfaces. In addition, conventional approaches to mitigate scaling, such as inhibitor addition have so far proven less effective against silica scaling (Demadis et al., 2007). Although precipitation of amorphous silica in natural geothermal settings has been studied extensively (e.g. Mountain et al., 2003; Tobler et al., 2008), the processes that occur at the fluid-equipment interfaces are not well understood. One of the complicating factors is corrosion of the pipes and other fluid handling equipment that are usually made of various types of steel. Corrosion can affect scaling, resulting in silica scales enriched in iron and/or containing inclusions of iron or other metal sulfides or oxides (Deutscher et

al., 1980; Rothbaum et al., 1979). Furthermore, corrosion can also enhance precipitation due to the creation of higher surface areas (Harrar et al., 1982; Neofotistou and Demadis, 2004). In high enthalpy geothermal systems, corrosion is usually a consequence of the reactions between corrosive dissolved gas (most often hydrogen sulfide, $H_2S_{(aq)}$ e.g. ~20 ppm of $H_2S_{(aq)}$ in the separated water at the Hellisheiði power plant; Meier et al., 2014) and metal surfaces. This reaction most often leads to the formation of metal sulfides. Under fully reducing conditions, studies in geothermal systems have shown that mackinawite (non-stoichiometric FeS) is the dominant mineral phase forming as a corrosion product (Soylemezoglu and Harper, 1982; Tang et al., 2010). Other iron sulfides such as greigite, troilite, pyrrhotite and pyrite have been observed under slightly more oxidized conditions. Under even more oxidizing conditions even iron (hydr)oxides (goethite, hematite, magnetite) have been observed (Richter et al., 2006; Soylemezoglu and Harper, 1982), although these could be simply an oxidation product of the former sulfides.

Scaling in geothermal systems, especially when occurring rapidly, can limit the extent of corrosion (Braithwaite and Lichti, 1980; Lichti et al., 1981). In a recent study, based on a single time point we (Meier et al., 2014) suggested that corrosion in the pipes of Hellisheiði occurred before the build-up of substantial silica layers. However, where more silica precipitation occurred corrosion was prevented or at least slowed down. If silica scaling could be controlled, this could potentially represent a cheap and easy way to reduce the issues related to corrosion in silica-rich geothermal systems. The problem however lies in the fact that, the mechanism and temporal relationships between scale formation and corrosion are still poorly quantified. With this study, we took the first step in this direction by evaluating the temporal changes in silica scaling and corrosion of carbon steel, deployed inside the pipelines at Hellisheiði for different periods of time (between 1 day and 10 weeks). Our results allowed us to quantify how rapid silica scaling occurred. We show that silica scaling resulted in the formation of a dense layer of amorphous silica that quickly isolated the steel surfaces from the reacting geothermal fluids. This way, in some cases, the silica cover strongly reduced and even prevented further corrosion.

MATERIALS AND METHODS

Silica precipitation and corrosion were monitored using stainless steel scaling plates (5 cm x 2 cm) deployed at four different points within the pipelines of the Hellisheiði geothermal power plant (Figure 1): (1) inside the power plant but before the heat exchangers, (2) inside the power plant but after the heat exchangers, (3) outside the power plant and (4) at the Húsmúli injection site, after mixing with steam condensate. All these deployment points were located in pipes that carried fluid following steam separation for use in the production of electrical energy. After the removal of the steam the separated water reached supersaturation with respect to amorphous silica and precipitation occurred. The four locations differed with respect to temperature, fluid flow rate and concentration of dissolved silica and H_2S_{aq} (Table 1).

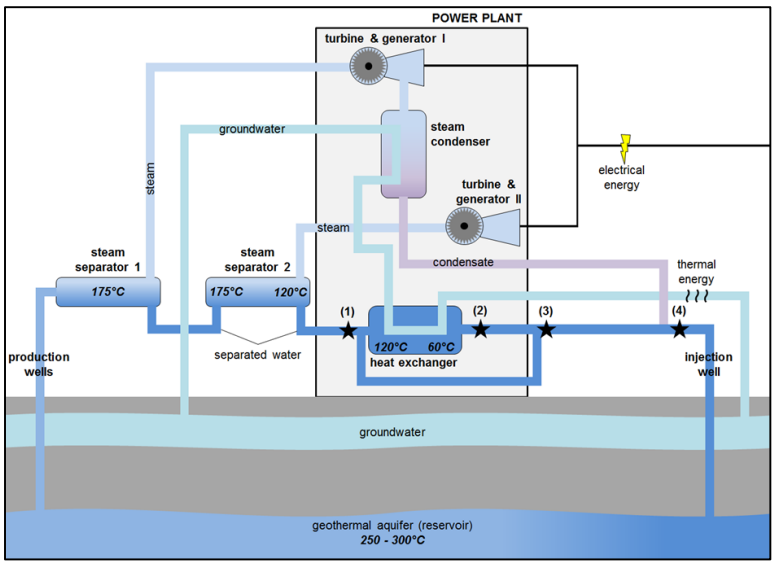

Figure 1: Schematic of the Hellisheiði geothermal power station indicating the four locations (*) at which the scaling plates were immersed. Full details and schematics of the Hellisheiði power plant are available at http://www.or.is/vinnsluras.

At each location two scaling plates (wiped clean with ethanol and stored in individual tubes until deployment) were inserted into pipes into the fast (up to 400 liters/second) flowing fluid. The bottom plate was a S316 stainless steel plate (Figure 2A, left), while the top plate consisted of an equivalent S316 stainless steel plate onto which 3 different 2 x 1.3 cm coupons were glued (Fig. 2A, right) using Loctite Hysol 9455 epoxy adhesive. These coupons were used to assess the effects that varying substrate composition and surface roughness have on silica precipitation and corrosion. The coupons consisted of (a) tachylite from south Iceland, (b) opal from Coober Peedy, Australia and (c) S275 carbon steel (Figure 2A at right). In the current paper we focus primarily on the processes observed on the S275 carbon steel coupons and compared them with the results from the S316 stainless steel plates. All other substrates are part of another publication (van den Heuvel et al., in prep.). The S275 carbon steel contained 0.25 % carbon, 1.6% manganese, 0.05% silicon, 0.04% phosphorus and 0.05 % sulfur.

Each set of scaling plates was deployed for between 1 day and 10 weeks. At the beginning and end of each deployment, the separated water was sampled at each location through a valve and immediately filtered through 0.2 µm polycarbonate filters. The pH was measured at temperatures of 23 to 27 °C and sample aliquots were collected for analysis of anions, cations and dissolved gases (for details of sample preservation and sampling containers see Arnórsson et al., 2006). The *in-situ* fluid temperatures at each location were obtained from the power plant operators. Anions were analyzed by ion chromatography (IC) and cations by inductively coupled plasma-mass spectrometry (ICP-MS) at the University of Leeds. The concentration of dissolved gases was measured by titration at Reykjavik Energy according to the methods described by Arnorsson et al. (2006). The filters were retained, dried and the solids on the filters analyzed by X-ray diffraction (XRD, Bruker D8, CuKα_1; 5-90° 2θ, 0.01°/step) at the University of Leeds. XRD patterns were evaluated using the EVA software (Bruker, Version 3.0). The compositions of the separated waters, as well as the pH and temperatures were used as inputs for geochemical simulations with PHREEQC (version 3.0, Parkhurst and Appelo, 2013) using the database phreeqc.dat updated with the latest thermodynamic data for amorphous silica (Gunnarsson and Arnórsson, 2000).

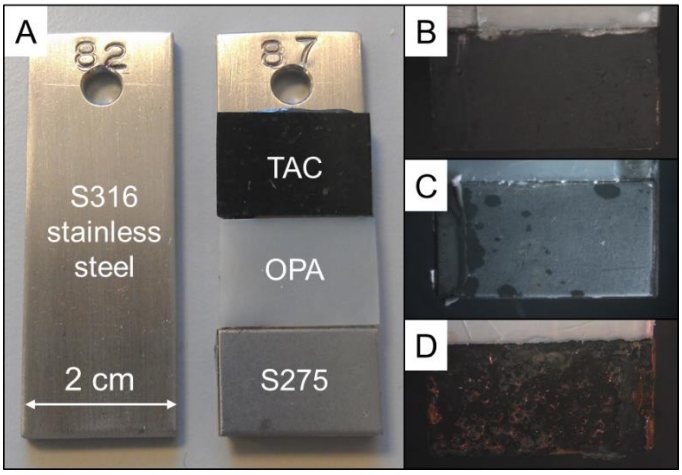

Figure 2: Photographs of scaling plates before (A) and after the deployments (B-D). For each deployment, two scaling plates were prepared (A): S316 stainless steel scaling plate (left) and S316 stainless steel scaling plate with tachylite (TAC), opal (OPA) and carbon steel (S275) coupons glued onto its surface (right). During some deployments, the carbon steel corroded showing homogeneous blackening (B), patchy corrosion (C) or the formation of a thick layer of corrosion products (D).

After set periods of time the plates were removed from the fluid and dried at 30°C for 24 h. They were photographed and where possible, precipitates and/or corrosion products from half of each scaling plate or coupon were scraped off with a plastic spatula. These materials were ground using an agate mortar and pestle and the powders analyzed by XRD as described above. All plates were then coated with ~40 nm of gold and the precipitates or corrosion features were imaged using a field emission scanning electron microscope (FEG SEM, FEI Quanta 650 at 20 keV). Spot analyses were performed using an energy dispersive spectrometer (EDS) and spectral information evaluated using the AZtec software (Oxford Instruments, Version 2.2). The SEM images were used to determine the size of the observed morphological features by measuring at least 100+ individual features on each coupon or plate manually and determining their mean dimensions.

RESULTS

Composition of geothermal fluid

The sampling locations differed with respect to the fluid temperature, composition of the separated water and thus pH and Eh (Table 1). The temperatures decreased from 118°C before the heat exchanger (location1) to just under 60°C at locations 2 and 3. The fluid composition was more or less constant with ~800 ppm SiO_2 and nearly 400 ppm NaCl for these three locations. Dissolved gases were also abundant with around 25 ppm CO_2 and 20 ppm H_2S (Table 1). The measured fluid pH is identical for locations 1 to 3. However, the calculated pH using PHREEQC is lower in all cases as it is re-calculated to reflect the *in-situ* temperatures. The difference in pH is biggest (nearly 1 log unit) at location 1 where the fluid is hottest and less than half a log unit at the cooler locations 2 and 3. The Eh is lower at the highest temperature (location 1) and similar at all other locations. Location 4 was different due to the addition of steam condensate (Figure 1). The condensate was hotter than the separated water (just over 70°C) and its addition lead to dilution of the SiO_2 and H_2S concentrations (~ 550 ppm and 14 ppm respectively; Table 1). The calculated pH and Eh values fell in between those of the other locations (8.8 and -0.5 respectively, Table 1). Overall, location 1, 2 and 3 were fairly similar yet, location 4 was by far the most diverse in terms of temperature, pH, Eh and fluid composition.

Table 1: Average and standard deviation of measured temperatures, fluid compositions and pH and calculated pH and Eh for each sampling location.

		Loc. 1	Loc. 2	Loc. 3	Loc. 4
Temp.	[°C]	117.8 ± 0.4	56.6 ± 1.6	58.0 ± 5.3	72.5 ± 11.2
CO_2	[ppm]	25.4 ± 5.5	25.2 ± 4.8	23.8 ± 3.7	18.5 ± 3.8
H_2S	[ppm]	19.2 ± 2.9	19.8 ± 2.5	20.5 ± 1.9	14.3 ± 2.7
SiO_2	[ppm]	802 ± 19	801 ± 30	794 ± 30	550 ± 76
Na	[ppm]	204 ± 8	205 ± 9	207 ± 8	140 ± 10
Cl	[ppm]	173 ± 12	171 ± 9	175 ± 6	120 ± 5
K	[ppm]	34.7 ± 1.6	34.7 ± 1.7	35.1 ± 1.6	23.6 ± 1.2
Al	[ppm]	1.99 ± 0.09	2.04 ± 0.11	2.04 ± 0.11	1.36 ± 0.07
Ca	[ppm]	0.71 ± 0.13	0.70 ± 0.06	0.71 ± 0.04	0.50 ± 0.06
Fe	[ppb]	28.5 ± 44.5	16.4 ± 13.1	21.6 ± 23.5	25.2 ± 29.5
Mg	[ppb]	21.5 ± 21.5	19.6 ± 12.9	19.7 ± 14.2	22.1 ± 15.6
pH meas. [1)]		9.4 ± 0.2	9.4 ± 0.2	9.4 ± 0.2	9.1 ± 0.3
pH calc.[2)]		8.5 ± 0.1	9.0 ± 0.1	9.0 ± 0.1	8.8 ± 0.2
Eh[2)]	[V]	-0.56 ± 0.01	-0.46 ± 0.01	-0.47 ± 0.01	-0.48 ± 0.02
Amorphous silica					
Solubility [3)]	[ppm]	470	210	210	260
Saturation index [2)]		0.1	0.4	0.4	0.2

[1)] As measured at 23 to 27 °C

[2)] Derived from PHREEQC simulations at *in-situ* temperatures and with the given fluid compositions

[3)] Calculated according to Gunnarsson and Arnorsson (2000)

Electron microscopic images of the materials captured by the filters revealed the presence of spherical particles, which at locations 1 to 3 varied in size between 0.05 and 25 µm (0.3 to 0.7 µm on average). EDS identified these as silica. In

addition, small platy phases on the filters were identified by EDS analyses to primarily consist of Al and Si and complementary XRD analyses suggested these to be the alumosilicate clinochlor. At location 4, such silica particles were very sparse, but platy alumosilicates were abundant. XRD identified them as chamosite and clinochlore and the magnesium silicate sepiolite. At all locations, on the filters we also found small (<2 μm) metal rich (identified by EDS) flakes, which were transported along in the fluid and likely originated from the corrosion of the pipelines or valves.

Description of mineral phases and corrosion features on scaling plates

We compare here features observed on the S316 scaling plates and the S275 coupons from each location with immersion times of 1 day, 1 week, 2 weeks, 4 weeks, 6 weeks and 10 weeks. At location 2, all glued on S275 carbon steel coupons were lost during deployments. At the remaining three locations, all but one (location 3, 1 week) S275 carbon steel coupons were recovered (Table 2).

At location 1, regardless of deployment time no or only minor macroscopically distinguishable traces of corrosion were visible (Table 2) on the S275 carbon steel coupons. Microphotographs however, revealed that the coupon surfaces were largely covered by an uneven layer of amorphous silica (identified by XRD) that consisted primarily of rounded 'bumps' and individual spherical silica particles (Figure 3A&B). The diameter of these 'bumps' increased from 0.3 μm after 1 day to over 12 μm after 10 weeks (Figure 3A&B , Figure 4A). This is identical to the change in size of amorphous silica 'bumps' determined on the stainless steel plates from the same location (van den Heuvel et al., in prep.). In addition, silica microspheres identical to those observed on the filters were found on the silica-coated steel surfaces (Figure 3A). Furthermore, variably shaped corrosion minerals (needles, flowers, blades plates), were found to break through the silica layers in some places (Figure 3C- E). Due to this localized appearance, the exact nature of these mineral phases could not be identified by XRD. However, their morphologies together with multiple EDS spot analyses (solely Fe and, in most cases, S) and combined with the bulk XRD confirmed these phases to be iron sulfides (mackinawite and greigite) and their oxidation products (the iron oxides hematite and goethite).

The S275 carbon steel coupons recovered from location 3 were more intensely corroded compared to location 1 with two of the plates completely and homogeneously blackened and two more showing patchy corrosion (Figure 2B). However, microscopically only sample 3-1d showed abundant corrosion features with dense or bladed mineral habits covering the coupon surface (Figure 3C-E). These corrosion minerals were similar to location 1 (iron sulfides and its oxidation products). Most other recovered coupons at location 3 were absolutely free of corrosion features even at the microscopic level. They were however, all characterized by the same uneven, bumpy, amorphous silica layer as in location 1. The individual 'bump' diameters increased from 0.2 μm after 1 day to over 5 μm after 10 weeks (Figure 3A&B, Figure 4B). Similar to location 1, some amorphous silica microspheres were also observed on top of the continuous silica layers.

Table 2: Stereo microscope (black) and scanning electron microscopy (in grey) observations of corrosion features and shapes of products. At locations 1 and 3 an uneven silica layer was the dominant precipitate.

	Loc. 1	Loc. 3	Loc. 4
1 day	no corrosion needles, bladed, platy	homogeneous[1)] dense, bladed	patchy[2)] tubular, bladed
1 week	no corrosion needles, bladed	– –	homogeneous tubular, bladed, platy
2 weeks	patchy only silica	patchy only silica	continuous layer[3)] blistered, dense
4 weeks	no corrosion needles	no corrosion needles	homogeneous tubular, bladed, flowers
6 weeks	patchy flowers	homogeneous only silica	continuous layer blistered, dense
10 weeks	no corrosion needles	patchy only silica	continuous layer blistered, dense, bladed

[1)] Homogeneous blackening of the steel coupon without a noticeable increase in thickness and no apparent change in surface texture (Figure 2B)

[2)] Individual dark to orange patches surrounded by (macroscopically) uncorroded steel (Figure 2C)

[3)] Formation of a dark brown to orange continuous layer with a noticeably increased thickness and a much more irregular surface compared to the S275 steel (Figure 2D)

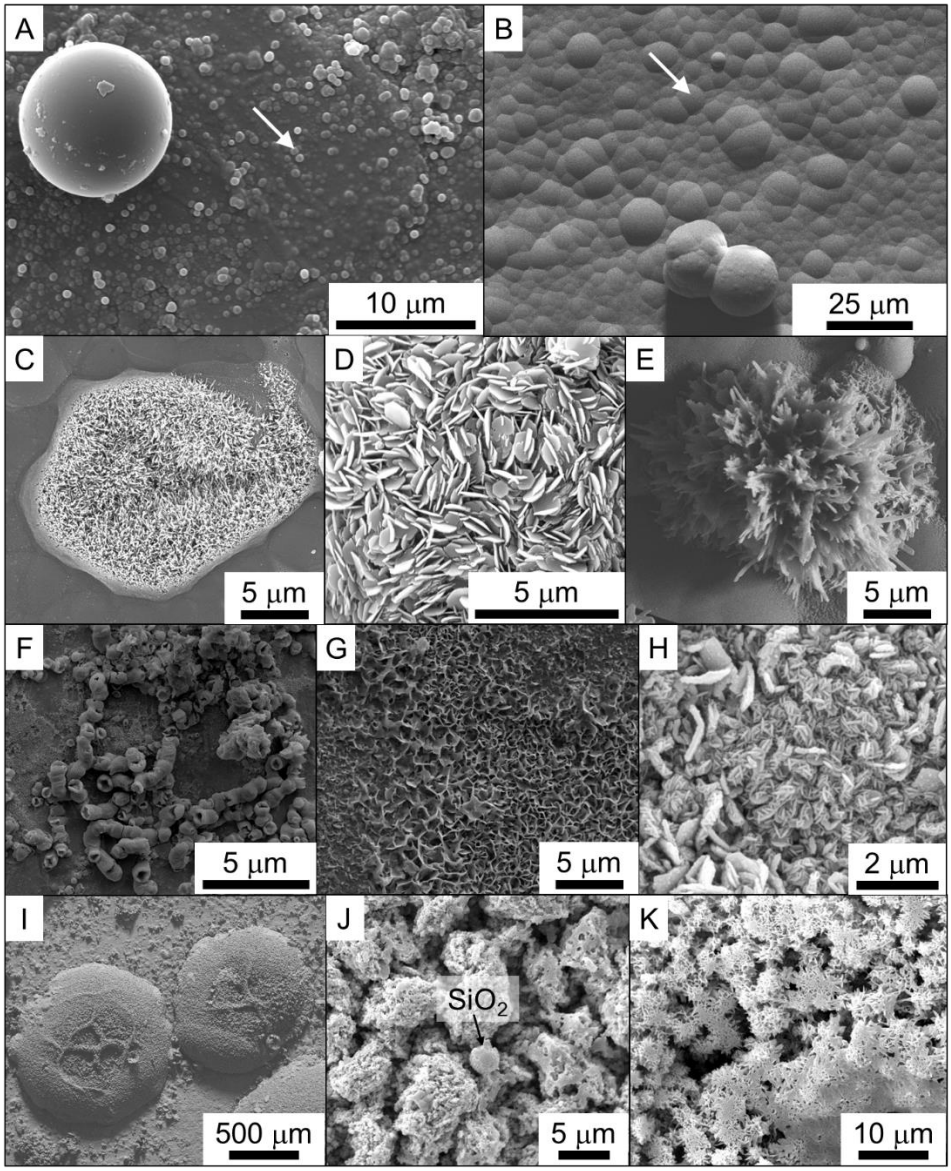

Figure 3: SEM microphotographs of amorphous silica textures and corrosion morphologies observed on the S275 carbon steel coupons. At locations 1 the plates were dominated by an uneven layer of amorphous silica with the size of individual 'bumps' (arrows) increasing over time (A = 1 day & B = 6 weeks). Individual spherical silica particles between 0.5 to 25 μm were also often seen (A & B). At location 3 both, the silica 'bumps' and the individual particles were slightly smaller. Variously shaped Fe-sulfides and/or oxides (EDS, not shown) were found: needle-shaped (C), platy (D) or flower-shaped habits (E). At location 4, corrosion was dominant and expressed as two main textures: homogeneous blackening of the steel and formation of a thick layer of corrosion products consisting of tubular structures (F) surrounded by bladed (G) and platy crystals (H) of Fe-sulfides and/or –oxides. The thick corrosion layers all showed blistering (I) and the formation of dense (J) Fe-sulfides and/or –oxides. Flower- or rosette-shaped aggregates (K) were encountered less frequently. No silica scaling 'bumps' and very few silica spheres (arrow in J) were observed at location 4.

Finally, on the coupons from location 4 totally different surface features were observed. All S275 carbon steel coupons showed clear and ubiquitous signs of corrosion. This includes the complete blackening of the carbon steel as well as the formation of thicker (estimated to be up to 0.5 mm), black and dark orange-brown corrosion layers (Figure 2B-D). On all samples characterized by homogeneous blackening of the carbon steel, tubular structures (Figure 3F) composed of aggregates of bladed crystals were observed. In-between these structures, the coupon surfaces was covered by bladed and platy crystals (Figures 3G&H). The thick corrosion layers were characterized by large (up to 2 mm) blister-shaped structures (Figure 3I) that consisted of dense aggregates and, more rarely, of flower- or rosette-shaped minerals (Figure 3J&K). The minerals that formed these corrosion layers were mackinawite (FeS), greigite (Fe_3S_4), hematite (Fe_2O_3), goethite (FeOOH) and elemental sulfur as confirmed not just through their morphologies but also through EDS analyses and XRD bulk analyses. Amorphous silica, the

dominant component at locations 1 and 3 was largely absent. Occasionally, spherical silica particles several micrometers in size were found incorporated into the corrosion layers (Figure 3J).

DISCUSSION

Mineral scaling

At locations 1 to 3, even after 1 day rapid silica scaling resulted in the complete coverage of the scaling plates and coupons. As predicted by PHREEQC calculations the solutions were all supersaturated with respect to amorphous silica. The saturation indices (SI) varied between 0.1 at location 1, 0.4 at locations 2 and 3 and 0.2 at location 4. Thus, theoretically, the scaling potential was lowest at location 1. However, the faster increase in 'bump' diameters at location 1 compared to location 3 indicated that the rate of silica deposition at this location was higher. This could be due to the elevated temperature (nearly 120 °C), which, despite increasing solubility, results in enhanced deposition of monomeric silica, i.e. growth (Gunnarsson and Arnórsson, 2003; Makrides et al., 1980; Tobler and Benning, 2013). The almost fully absent silica at location 4 is attributed to the more dilute conditions and thus much lower silica concentration (~550 pm) and the prevalence of corrosion at this location.

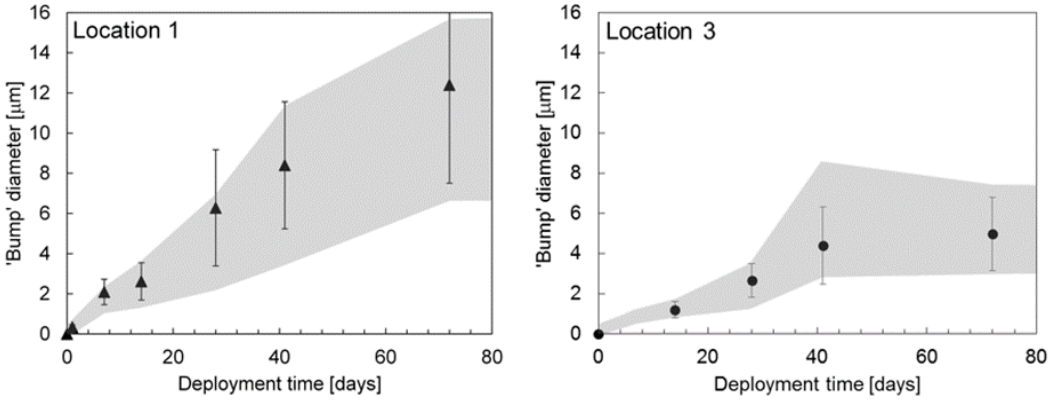

Figure 4: Increase of 'bump' diameters on the S275 stainless steel coupon as a function of time at location 1 (left) and location 3 (right). The data points correspond to the average diameters of 100+ individual 'bumps', while the error bars correspond to the standard deviations. The grey surfaces shown the average 'bump' diameter ± standard deviation as determined from the S316 stainless steel plates (van den Heuvel et al., in prep). The overlap between the date from S275 steel coupons and the S316 steel plates indicate that the growth of the silica scaling layers was independent of the underlying steel surface properties.

Silica can be deposited from a supersaturated solution by two pathways: molecular deposition and particle deposition (Weres et al., 1981; van den Heuvel et al., in prep.). Molecular deposition is the direct deposition of silica monomers (and potentially small polymers) onto a surface. This process results in the formation of the uneven surfaces consisting of adjoined silica 'bumps' with sizes that increase as a function of time. The increase is faster in the initial stages of precipitation (up to ~ 40 days) and seemingly slows down as time progresses (Figure 4). The similar shapes in the growth profiled between the 'bumps' formed on the S316 stainless steel plates (Figure 4, shaded areas) and those formed on the S275 carbon steel coupons (Figure 4, data points) suggests that under the conditions studied here the surface properties of the steel substrates have no effect on molecular deposition. Particle deposition requires the formation of silica particles by homogeneous nucleation first (Iler, 1979; Tobler et al., 2009; Tobler and Benning, 2013). Once such silica nanoparticles form in solution they can be deposited onto any available surface (Figure 3A&B) or remain in the fluid where they can grow further by a naturally occurring "buildup" (Mindick and Vossos, 1970) in which silica nanoparticles present in the fluid grow by Ostwald ripening through the constant addition of monomeric and polymeric silica. If deposited, the particles are cemented to the underlying surface or other particles by the continual coalescence through the amply available aqueous monomeric silica (Meier et al., 2014). Together, these two mechanisms make up the silica scales observed. Based on the scantiness of individual silica particles on the plates compared to the silica deposited in the 'bumps' we suggest that molecular deposition is the dominant mechanisms responsible for the bulk of the silica scales formed on the plates and coupons (van den Heuvel et al., in prep.).

Corrosion of the S275 carbon steel coupons

Dissolved gases are the primary corrosion species in geothermal fluid. At Hellisheiði, the following species could potentially be involved in the corrosion of the S275 carbon steel: dissolved oxygen, carbon dioxide ($CO_{2(aq)}$) and hydrogen sulfide ($H_2S_{(aq)}$). Based on the measured fluid compositions and temperatures, Eh values of -0.45 to -0.6, were obtained by PHRREQC, indicating strongly reducing conditions and negligible concentration of dissolved oxygen *in-situ*. However, a recent study Richter et al. (2007) showed that operational changes and maintenance procedures can result in a sudden increase in dissolved oxygen concentrations in certain parts of the pipelines, leading to rapid localized corrosion. Therefore, some corrosion caused by dissolved oxygen cannot be excluded, especially during the longer deployments. The second corrosion species present at Hellisheiði is carbon dioxide (CO_2). When dissolved in water it forms carbonic acid (H_2CO_3) which can then interact with the steel surface to oxidize iron and precipitate siderite ($FeCO_3$) (Mundhenk et al., 2013). The absence of siderite and the high pH of the fluids (Table 1) indicates that this corrosion mechanism did not take place inside the pipelines at Hellisheiði. The predominant corrosion products were sulfides resulting from the interactions between the carbon steel surfaces and the ~ 20 ppm dissolved hydrogen sulfide (Table 1).

The anoxic conditions in the pipelines of Hellisheiði suggested that the only iron sulfide to form should be mackinawite (Benning et al., 2000). Mackinawite formed as a corrosion product due to the interaction of the $H_2S_{(aq)}$-rich fluids and the steel coupons during the prolonged exposure of the coupons to the geothermal fluids. The second iron sulfide identified, greigite, is a common intermediate in the usually rapid transformation of mackinawite to pyrite (Benning et al., 2000; Hunger and Benning, 2007). This transformation when occurring fast can also result in the formation of elemental sulfur (Benning et al., 2000). However, in order to transform mackinawite to greigite, slightly oxic conditions are needed. We identified two possible scenarios:

(1) Any change in operating conditions or maintenance during prolonged exposure of the coupons could result in the introduction of short pulses of increased dissolved oxygen into the geothermal fluid (Richter et al., 2006) This oxygen would lead to the rapid transformation of mackinawite into greigite as shown by Cahill et al. (2000) and Csákberényi-Malasics et al. (2012) with elemental sulfur as a by-product (Benning et al., 2000). Once the conditions return to anoxic, the transformation would be stopped, and mackinawite would continually precipitate.

(2) The transformation of mackinawite to greigite only takes place when the steel coupons are removed from the fluid. Although the coupons were immediately placed into centrifuge tubes and sealed after sampling, they were not kept strictly anaerobic. As the transformations of mackinawite occurs extremely fast in oxic conditions, it is possible that the partial transformation of mackinawite to greigite took place in the thin film of water covering the coupons upon removal from the geothermal fluids and before drying.

Both scenarios could also lead to the formation of the observed iron (hydr)oxides goethite and hematite. However, these minerals could also have formed during aerobic sample storage and analyses. Nevertheless, the fact that both, mackinawite and greigite were still present in the samples clearly indicated that upon oxidation of the upper most layer of iron sulfides, the oxidation products hematite and goethite seemingly formed a protective layer thus preserving the original iron sulfides even under ambient conditions and over time periods of weeks to months although mackinawite and greigite are not stable at ambient aerobic conditions (Benning et al., 2000).

Scaling vs. corrosion

When both, scaling and corrosion occur at the same location concurrently, they invariably will affect each other. The formed corrosion products influenced the precipitation of amorphous silica in that it changed the morphology and properties of the steel coupon surface. Harrar et al. (1982) found that this resulted in faster initial scale formation onto mild steel compared to inert surfaces such as Teflon or the superalloy Hastelloy. The authors did not discuss the reasons for this observation. However, they inferred that the higher surface area of the corrosion phases likely resulted in higher molecular deposition rates as well as making the trapping of colloidal silica more likely. For longer exposure times and higher scaling rates the effect disappeared (Harrar et al., 1982). This is in line with the findings of this study, where we showed that when silica scaling dominates (i.e., locations 1 and 3), the scaling onto partially corroded S275 carbon steel is identical to the scaling observed onto S316 stainless steel (Figure 4 data points compared with grey areas).

Conversely, the precipitation of silica can impact the corrosion of the metal surfaces and this has been shown in several power plants (Braithwaite and Lichti, 1980; Lichti et al., 1981; Meier et al., 2014). When silica scales form fast, they can act as a barrier, isolating the steel surfaces from the fluid. The dense structure of such silica scales will subsequently impair fluid transport through the silica layer and slow down and potentially inhibit further corrosion. This is evidenced in the samples from location 1 where, based on the concentration of H_2S and the fluid temperature, corrosion rates should be highest.

However, only limited corrosion was observed at location 1 even after 10 weeks. Similarly, at location 3, which although at lower temperatures was characterized by almost identical chemical conditions, corrosion was limited (Table 2). Only few coupons at location 3 showed macroscopic signs of uniform or patchy corrosion but when observed at high resolution no obvious corrosion products were seen. This indicates that, at least in some cases, corrosion likely took place immediately after immersion of the coupons and before the initial stages of silica precipitation and that any continual corrosion was stopped or slowed once a complete layer of silica covered the coupons. Finally, the biggest difference was observed for the coupons deployed at location 4, where the silica precipitation is less important (van den Heuvel et al., in prep.), and thus corrosion dominated because a protective silica layer was absent. As a consequence, the corrosion of the S275 carbon steel was much more uniform and extensive, sometimes even forming thick layers of iron phases when deployed for longer times (Table 2; Figure 2D).

CONCLUSION

Concurrent mineral scaling and corrosion processes have been observed in geothermal systems before but up to date only a small number of studies have evaluated the relationship between these two processes. By characterizing the temporal relationship between silica scaling and corrosion at the Hellisheiði power station we demonstrate that both, scaling and corrosion took place within a day of placing the scaling plates into the geothermal fluid. Where silica scaling was rapid (locations 1 and 3), corrosion was very limited to non-existent, while at location 4, where silica precipitation is less important, corrosion of the S275 steel is the dominant process.

Our data shown that where silica scaling passivates exposed surfaces, it can prevent or at least drastically reduce corrosion of steel surfaces. Such fast silica scaling could thus represent a means to protect steel surfaces susceptible to corrosion in a cheap and fast way. However, silica scaling in geothermal power plants is inherently difficult to control and so far none of the employed approaches such as pH modification, dilution, controlled polymerization and/or precipitation as well as the use of (in)organic inhibitors allowed for a universally applicable mitigation strategy to be developed. Furthermore, even if perfect control of amorphous silica precipitation would be feasible in the future, the problem of localized corrosion associated with uneven steel surfaces or cracks in the precipitation layer for further fluid attach remain.

Although our work has advanced our understanding of the inter-dependencies between silica scaling and metal corrosion, the challenge for the future remains to see if controlled silica scaling may become a possible strategy to deal with corrosion of steel surfaces in high-enthalpy geothermal power plants.

REFERENCES

Arnórsson, S., Bjarnason, J.Ö., Giroud, N., Gunnarsson, I., Stefánsson, A., 2006. Sampling and analysis of geothermal fluids. *Geofluids* **6**, 203-216.

Benning, L.G., Wilkin, R.T., Barnes, H., 2000. Reaction pathways in the Fe–S system below 100 C. *Chemical Geology* **167**, 25-51.

Braithwaite, W., Lichti, K., 1980. Surface corrosion of metals in geothermal fluids at Broadlands, New Zealand. *Geothermal Scaling and Corrosion, ASTM STP* **717**, 81-112.

Cahill, C., Benning, L., Barnes, H., Parise, J., 2000. In situ time-resolved X-ray diffraction of iron sulfides during hydrothermal pyrite growth. *Chemical Geology* **167**, 53-63.

Csákberényi-Malasics, D., Rodriguez-Blanco, J.D., Kis, V.K., Rečnik, A., Benning, L.G., Pósfai, M., 2012. Structural properties and transformations of precipitated FeS. *Chemical Geology* **294**, 249-258.

Demadis, K.D., Mavredaki, E., Stathoulopoulou, A., Neofotistou, E., Mantzaridis, C., 2007. Industrial water systems: problems, challenges and solutions for the process industries. *Desalination* **213**, 38-46.

Deutscher, S., Ross, D., Quong, R., Harrar, J.E., 1980. Studies of the dissolution of geothermal scale. California Univ., Livermore (USA). Lawrence Livermore Lab.

Gunnarsson, I., Arnórsson, S., 2000. Amorphous silica solubility and the thermodynamic properties of H 4 SiO 4 in the range of 0 to 350 C at P sat. *Geochimica et Cosmochimica Acta* **64**, 2295-2307.

Gunnarsson, I., Arnórsson, S., 2003. Silica scaling: The main obstacle in efficient use of high-temperature geothermal fluids, International Geothermal Conference, Reykjavik, pp. 30-36.

Harrar, J., Locke, F., Otto Jr, C., Lorensen, L., Monaco, S., Frey, W., 1982. Field tests of organic additives for scale control at the Salton Sea geothermal field. *Society of Petroleum Engineers Journal* **22**, 17-27.

Hunger, S., Benning, L.G., 2007. Greigite: a true intermediate on the polysulfide pathway to pyrite. *Geochem. Trans* **8**, 1.

Iler, R.K., 1979. The chemistry of silica: solubility, polymerization, colloid and surface pro perties, and biochemistry. Wiley.

Lichti, K.A., Soylemezoglu, S., Cunliffe, K.D., 1981. Geothermal corrosion and corrosion products, *Proceeding of the New Zealand Geothermal Workshop*, pp. 103-108.

Makrides, A.C., Turner, M., Slaughter, J., 1980. Condensation of silica from supersaturated silicic acid solutions. *Journal of Colloid and Interface Science* **73**, 345-367.

Meier, D.B. (now van den Heuvel), Gunnlaugsson, E., Gunnarsson, I., Jamtveit, B., Peacock, C., Benning, L., 2014. Microstructural and chemical variation in silica-rich precipitates at the Hellisheiði geothermal power plant. *Mineralogical Magazine* **78**, 1381-1389.

Mindick, M., Vossos, P.H., 1970. Large particle silica sols and method of production. *Google Patents*.

Mountain, B., Benning, L., Boerema, J., 2003. Experimental studies on New Zealand hot spring sinters: rates of growth and textural development. *Canadian Journal of Earth Sciences* **40**, 1643-1667.

Mundhenk, N., Huttenloch, P., Sanjuan, B., Kohl, T., Steger, H., Zorn, R., 2013. Corrosion and scaling as interrelated phenomena in an operating geothermal power plant. *Corrosion Science* **70**, 17-28.

Neofotistou, E., Demadis, K.D., 2004. Use of antiscalants for mitigation of silica (SiO 2) fouling and deposition: fundamentals and applications in desalination systems. *Desalination* **167**, 257-272.

Parkhurst, D.L., Appelo, C., 2013. Description of input and examples for PHREEQC version 3: a computer program for speciation, batch-reaction, one-dimensional transport, and inverse geochemical calculations. US Geological Survey.

Richter, S., Hilbert, L.R., Thorarinsdottir, R., 2006. On-line corrosion monitoring in geothermal district heating systems. I. General corrosion rates. *Corrosion science* **48**, 1770-1778.

Richter, S., Thorarinsdottir, R., Jonsdottir, F., 2007. On-line corrosion monitoring in geothermal district heating systems. II. Localized corrosion. *Corrosion science* **49**, 1907-1917.

Rothbaum, H., Anderton, B., Harrison, R., Rohde, A., Slatter, A., 1979. Effect of silica polymerisation and pH on geothermal scaling. *Geothermics* **8**, 1-20.

Scott, S., Gunnarsson, I., Arnórsson, S., Stefánsson, A., 2014. Gas chemistry, boiling and phase segregation in a geothermal system, Hellisheidi, Iceland. *Geochimica et Cosmochimica Acta* **124**, 170-189.

Soylemezoglu, S., Harper, R., 1982. Oxygen ingress into geothermal steam and its effect on corrosion of low carbon steel at Broadlands, New Zealand. *Geothermics* **11**, 31-42.

Tang, J., Shao, Y., Guo, J., Zhang, T., Meng, G., Wang, F., 2010. The effect of H 2 S concentration on the corrosion behavior of carbon steel at 90 C. *Corrosion Science* **52**, 2050-2058.

Tobler, D.J., Benning, L.G., 2013. In situ and time resolved nucleation and growth of silica nanoparticles forming under simulated geothermal conditions. *Geochimica et Cosmochimica Acta* **114**, 156-168.

Tobler, D.J., Stefansson, A., Benning, L.G., 2008. In-situ grown silica sinters in Icelandic geothermal areas. *Geobiology* **6**, 481-502.

van den Heuvel, D.B., Gunnlaugsson, E., Gunnarsson, I., Peacock, C.L., Benning, L.G., in prep.

Weres, O., Yee, A., Tsao, L., 1981. Kinetics of silica polymerization. *Journal of Colloid and Interface Science* **84**, 379-402.